PRAMANA
— journal of
physics

Vol. 42, No. 1,
January 1994
pp. 49–64

Optical design of a toroidal grating monochromator based beam line on Indus-1

K J S SAWHNEY and R V NANDEDKAR
Accelerator Program, Centre for Advanced Technology, Indore 452013, India

MS received 8 April 1993; revised 22 September 1993

Abstract. In this paper, we discuss the detailed optical design of a beam line that is under construction on the synchrotron radiation source, Indus-1. Toroidal mirrors are used as pre- and post- focusing elements and a toroidal grating monochromator as a dispersing element. Using three interchangeable gratings, this monochromator will give, at a moderate resolution, a good throughput on the sample in the wavelength range 40 to 1000 Å. Effect of various parameters and their optimization on the resolution and throughput characteristics have been studied by ray tracing calculations, and presented.

Keywords. Synchrotron radiation; beam line; soft X-ray; vacuum ultraviolet.

PACS No. 42·10

1. Introduction

The measurement of optical properties in vacuum ultraviolet (VUV) and soft X-ray regime (20–2000 Å) is an important area. The measurements in this entire wavelength regime can only be performed using a synchrotron radiation (SR) source. Various sources, detectors and spectrometers are generally required to be calibrated in this wavelength range. The optical constants, viz., the index of refraction and extinction coefficients need to be determined for various polarization components. For these investigations, high intensity monochromatic radiation in the above-mentioned wavelength range is required; however, the resolution requirement is moderate ($\lambda/\Delta\lambda \sim 500$). To carry out this type of studies preliminary design of a multipurpose beam line was conceived [1,2]. This beam line is being built for setting up on the 450 MeV Indus-1 synchrotron radiation source (SRS). The same beam line will be used for reflectometry to investigate optical constants of materials, multilayers etc in VUV and soft X-ray regime. The purpose of a beam line is to deliver monochromatic light onto a sample. The detailed optical design of this beam line is presented in this paper. The theoretical performance of the beam line has been evaluated using ray tracing calculations.

2. General considerations

In the wavelength range of our interest (40–1000 Å) reflecting optics predominates due to the high absorption of all materials in this wavelength region and the only useful optical elements with good imaging properties are the reflecting mirrors and reflection gratings. Furthermore, to achieve a sufficiently high reflectivity at gratings and mirrors, it is necessary to work at nearly grazing incidence. The imaging quality

deteriorates, however, at such grazing angles and even aspherical focusing elements give poor imaging for the off-axial points of an object. There are further problems which arise in this spectral range:

Gratings with high groove densities are needed in order to obtain high angular dispersion and thus high resolution. Such gratings are relatively inefficient and may generate a considerable amount of stray light.

Since SRS is a continuum source of radiation, higher order contributions from diffracting elements may be present and these have to be minimized. This is a severe problem because in general the SR is more intense at short wavelengths.

Aspheric surfaces with very good surface quality are difficult to manufacture.

Furthermore, since the source point is fixed in space, the optical system of the beam line has to be designed in such a way that a fixed exit beam is obtained. Also, to avoid build-up of contamination on the reflecting surfaces, the beam line has to be operated under ultra high vacuum (UHV) conditions. All these considerations have been taken into account in designing the beam line.

3. Optical design

In general, the optical components of a typical beam line consist of a premirror to collect and focus the incident radiation, a monochromator to select a wavelength of interest and a post-mirror to focus the monochromatic radiation onto the sample. We have designed a beam line based on a toroidal grating monochromator and its optical configuration is given in figure 1. Various considerations going into this design are described in the following.

3.1 *Source characteristics*

Indus-1 is a 450 MeV electron storage ring with four bending magnets [3]. A storage ring provides SR by the acceleration of relativistic electrons in the dipole magnetic field of the bending magnets. The radiation is emitted tangentially with 100% linear polarization in the plane of the orbit and is highly collimated in the vertical direction.

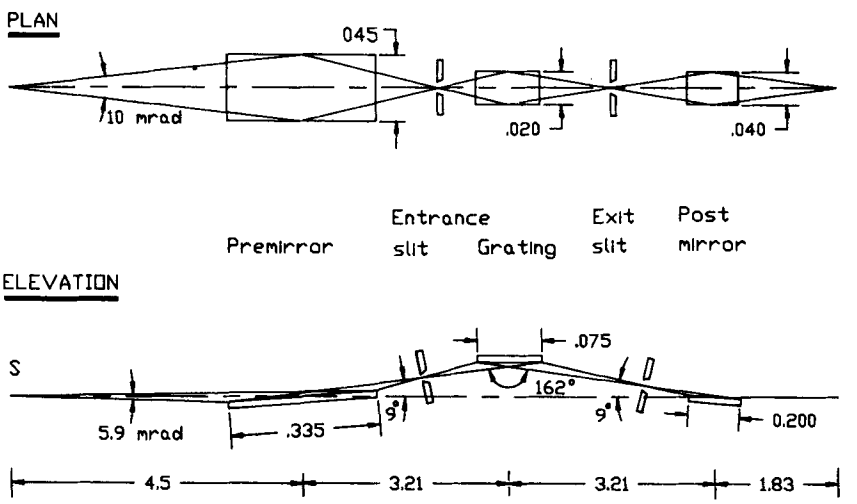

Figure 1. Optical layout of the beam line. All dimensions are in metres.

Table 1. Characteristics of Indus-1 synchrotron radiation source.

Electron energy	:	450 MeV
Source type	:	Bending magnet
Bending magnet radius	:	1000 mm
Critical wavelength	:	61 Å
Source size (σ)	:	0·8 mm × 0·1 mm
Horizontal divergence	:	10 mrad
Vertical divergence	:	2–5 mrad

The SR spectrum from Indus-1 consists of a quasi-continuum radiation with a critical wavelength of 61 Å. The SR source size is determined by the cross-section of the electron beam, which in turn depends on the emittance and the angle at which the SR is taken out from the bending magnet. We have considered high emittance mode and our beam line will be on a 10° port on the bending magnet [4]. For this case, the electron beam size is 0·1 mm vertically and 0·8 mm horizontally [5]. Furthermore, the height, width and vertical divergence are not sharply cut-off but follow gaussian distribution. The values quoted above are the σ values of these gaussian distributions. The vertical divergence of the SR beam is wavelength dependent and is given by:

$$\sigma_y = \frac{570}{\gamma}\left[\frac{\lambda}{\lambda_c}\right]^{0.43} \tag{1}$$

where γ is the electron energy measured in units of the electron rest mass and λ_c is the critical wavelength ($\gamma = 881$ and $\lambda_c = 61$ Å for Indus-1). The vertical divergence increases with increasing wavelength and it is typically in the range of 2–5 mrad. The horizontal divergence is limited by the vacuum port through which the radiation is extracted from the storage ring and for our beam line it is 10 mrad. The various parameters of Indus-1 employed by us for beam line design are given in table 1. The beam power intercepted by this beam line from Indus-1 will be small and hence cooling of the optical elements is not necessary.

3.2 *Pre- and post-focusing mirrors*

For focusing synchrotron radiation, there exists a large choice of mirrors [6]. The simplest option of using spherical mirrors introduces large aberrations at grazing incidence. To reduce these aberrations, aspheric surfaces have to be used for mirrors and gratings. An ellipsoid is an ideal surface to get a stigmatic image of a point source. However, it is rather difficult to fabricate ellipsoidal surfaces and hence they are expensive. An aspheric surface which is easy to fabricate compared to an ellipsoid is a toroid. A toroid is generated by rotating a circle of radius ρ in an arc of radius R. The principal radii of curvature of the toroid are chosen to be equal to those of the ellipsoidal mirror. The principal radii of curvature of the ellipsoidal at the vertex are given by

$$R = \frac{1}{ab}[r_1 r_2]^{3/2} \tag{2}$$

$$\rho = \frac{b}{a}[r_1 r_2]^{1/2} \tag{3}$$

Table 2. Parameters of the toroidal pre- and post-mirrors.

Parameters	Pre-mirror	Post-mirror
R(mm)	38236·5	23400·7
ρ(mm)	235·4	144·1
Angle of incidence (w.r.t. mirror surface)	4·5°	4·5°
Source to mirror distance (mm)	4500	1836
Mirror to focus distance (mm)	2250	1836
Demagnification ratio	2:1	1:1
Size (mm × mm)	335 × 45	280 × 40
Coating	gold/platinum	

where r_1 and r_2 are the object and image distances from the mirror surface and a and b are the semi major and semi minor axes of the ellipsoid. If ψ is the angle of incidence on the mirror surface then a and b are given by

$$a = \frac{r_1 + r_2}{2}, \tag{4}$$

$$b = \sqrt{r_1 \cdot r_2} \cdot \cos\psi. \tag{5}$$

It was shown earlier [7] that for small source size and small horizontal acceptance, the toroidal mirror produces almost as good an image as an ellipsoidal mirror does, and since toroidal surfaces are easier to fabricate we have chosen toroidal mirrors as pre- and post- focusing elements for our beam line. The parameters of these mirrors are given in table 2. Various considerations for choosing the shapes and sizes of these mirrors given in this table are discussed in § 3·4.

3.3 *Toroidal grating monochromator*

The most critical component in the beam line is the monochromator. Unfortunately, the required wavelengths are too long for crystal monochromators and though conventional normal incidence grating monochromators for SR have good stigmatic properties, they cannot be used in the soft X-ray region ($\lambda < 300$ Å). Grazing incidence monochromators are most suitable for operation in the desired wavelength range. Various grazing monochromators [8] are classified according to the type of diffraction grating employed. Monochromators using plane gratings comprise one category, those with spherical gratings a second category and those utilizing aspherical gratings (e.g. toroids) a third category. Every monochromator represents a compromise in acceptance, resolution, spectral range, photon flux and complexity of design [9]. A toroidal grating monochromator (TGM) is the simplest to realize and is characterized by very high efficiency, large collection aperture, moderate resolution and a simple wavelength scanning mechanism. We have chosen a grazing incidence TGM in our beam line design. A number of TGM based beam lines are in operation at the various SR facilities worldwide [10].

When the TGM is used in the fixed deviation geometry, i.e., in a configuration in which the deviation angle between the entrance and exit arms is constant, the grating

Table 3. Parameters of toroidal grating monochromator.

Entrance arm length (mm)	:	1000
Exit arm length (mm)	:	1414
Deviation angle	:	162°
Major radius (mm)	:	7977·0
Minor radius (mm)	:	182·3
Wavelength range		
Grating 1 (1800 grooves/mm)	:	40–120 Å
Grating 2 (600 grooves/mm)	:	120–360 Å
Grating 3 (200 grooves/mm)	:	360–1000 Å
Ruled area of the grating (mm^2)	:	75 × 20
Coating	:	gold/platinum

equation reduces to

$$Nk\lambda = 2\cos\theta \sin(\theta + \beta) \tag{6}$$

where $2\theta = \alpha - \beta$ is the included angle, α is the angle of incidence, β is the angle of diffraction, N is the groove density and k is the diffraction order. α and β are of opposite sign if on the opposite sides of the surface normal. The angle $(\theta + \beta)$ is the deviation of the diffracted ray from the zeroth order, i.e., it is the scanning angle. Equation (6) shows that the wavelength is proportional to $\sin(\theta + \beta)$, implying that a simple sine bar mechanism is sufficient for wavelength scanning.

We plan to use the grating in the first diffraction order since higher orders are not desirable as they require higher angular scan range (due to higher dispersion) which lead to higher aberrations resulting in a net loss of resolution. Also, positive order (exit arm > entrance arm) is preferred as it intercepts more SR with the same size of the grating. Therefore, our monochromator will have $k = +1$. A direct consequence of operating in positive first order at fixed deviation geometry is that a cut-off exists in the long wavelength end of the spectrum corresponding to $\alpha = 90°$ case and hence more than one grating is generally required to cover the full wavelength range.

The design of our beam line is based on a commercially available monochromator TGM1400. Various parameters of the monochromator-like grating radii, included angle 2θ, groove frequency N and object and image distances determines the performance of the monochromator [11]. For instance, the included angle 2θ determines the short wavelength limit of the spectral range. The monochromator chosen has an included angle $2\theta = 162°$, which is sufficiently large to get photons of wavelength 40 Å, and at the same time is as small as possible to reduce the focusing aberrations. Since the aberration corrections are effective in a limited wavelength range, more than one grating is required to be used to cover the full spectral range of interest. The TGM selected utilizes three toroidal gratings which can be interchanged *in situ* without breaking the vacuum. The various parameters of the monochromator are given in table 3.

3.4 *Optical layout*

The optical configuration of the beam line shown in figure 1 comprises of a pre mirror M_1, an entrance slit S_1, a toroidal grating T, an exit slit S_2 and a post mirror M_2. The TGM combines the dispersion and focusing in one optical element, thus minimizing the reflection losses in the system. The various physical constraints such as the length

of the front end, thickness of the radiation shielding, etc. restricts the placement of the first mirror M_1 not before 4000 mm from the tangent point of the storage ring. We have therefore kept the first optical element i.e. the pre-focusing toroidal mirror at a distance of 4500 mm from the source. This mirror is inclined at 4·5° to the horizontal plane and it illuminates the entrance slit S_1 by a 2:1 demagnification of the SR source. The grating in the TGM is vertically dispersing at a constant deviation of 162° and has a ruled area of 75 mm × 20 mm. After diffraction by the grating, the monochromatic light passing through the exit slit is deflected back to the horizontal plane (plane of the electron orbit in the storage ring) by a second toroidal mirror at 1:1 magnification which focuses the monochromatised light onto the sample placed at a distance of 1836 mm from the mirror.

The choice of dimensions of the optical elements can be made following several different criteria. Since we plan to use commercially available gratings having ruled area of 75 mm × 20 mm, this becomes our starting point for determining the pre- and post-mirror sizes. For an entrance arm length of 1000 mm, this size of the grating corresponds to a maximum acceptance of the grating of 11·7 mrad vertical × 20 mrad horizontal (corresponding to zeroth order light, $\alpha = -\beta = 81°$). To match this acceptance with a 2:1 demagnification of the pre-mirror, a toroidal mirror of size 335 mm × 45 mm is required. Similarly, to determine the post-mirror size, the vertical and horizontal divergences at the exit slit should be known. These divergence values depend on the acceptance and magnification of the grating. In the dispersive direction, both these quantities depend on wavelength and are given by

$$\sigma_v(\lambda) = \frac{l \cos \alpha}{r_1} \tag{7}$$

and

$$M_v(\lambda) = \frac{\cos \alpha}{\cos \beta} \cdot \frac{r_2}{r_1} \tag{8}$$

where $\sigma_v(\lambda)$ and $M_v(\lambda)$ are the grating acceptance and magnification in the vertical direction, l is the length of the grating and r_1 and r_2 are the entrance and exit arm lengths of the monochromator. From (7) and (8) vertical divergence values of 9·5 mrad and 11·9 mrad are obtained at the exit slit for wavelengths 40 Å and 120 Å, respectively, which are the two extreme wavelength limits of the 1800 grs/mm grating (the other two gratings will also yield the same divergence values). The size of the post-mirror has to be calculated for the larger divergence value which yields a value of 278 mm for the post-mirror length. In the non-dispersive (horizontal) direction the divergence and magnification of the grating are wavelength independent. While the horizontal acceptance of the grating is 20 mrad, the magnification is simply given by r_2/r_1. The horizontal divergence at the exit slit is therefore 14·14 mrad which yields a size of 26 mm for the post-mirror width. We have taken the post-mirror size to be 280 mm × 40 mm which is slightly more than the calculated value. This has been done for manufacturing ease [12].

4. Beam line performance

4.1 *Ray tracing*

To investigate the imaging properties of the beam line, we have carried out simulation studies using ray tracing calculations. The ray tracing calculations enable one to

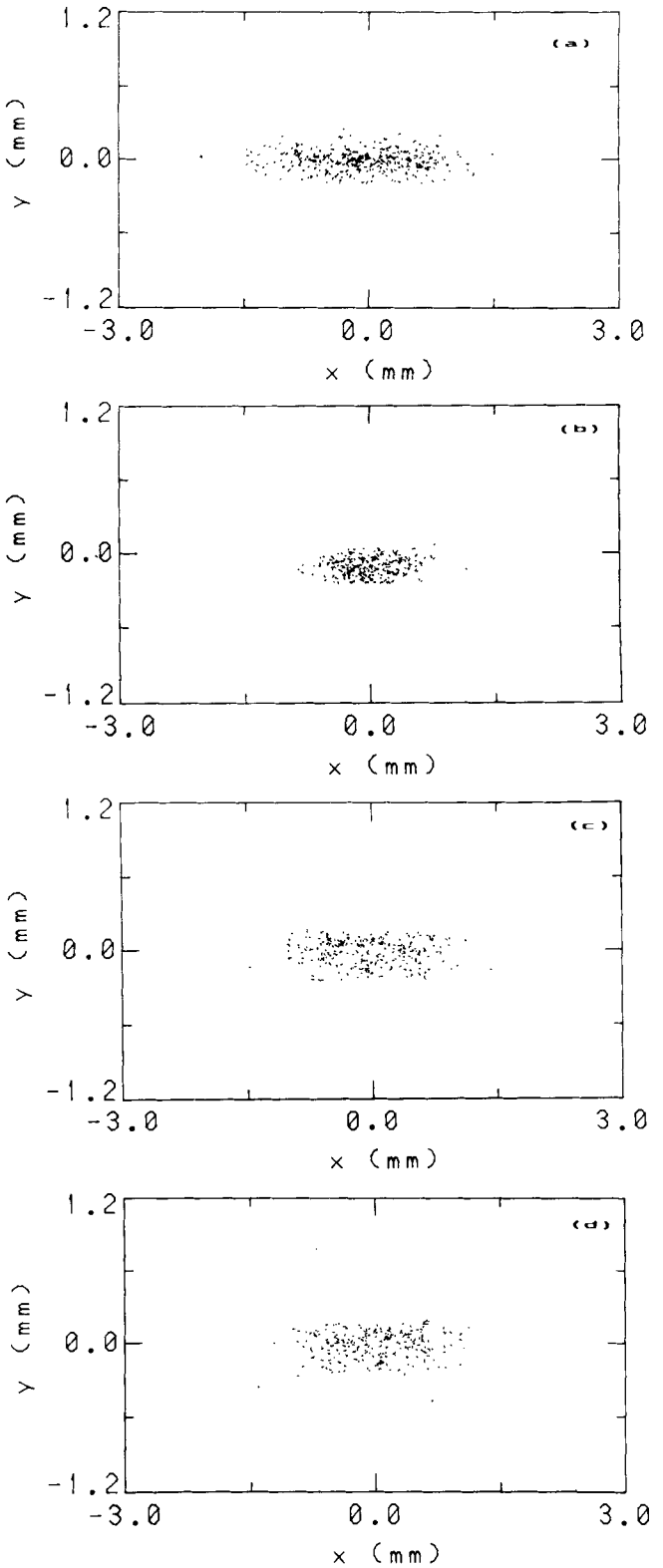

Figure 2. Intensity distribution at various focusing points: (**a**) Source, (**b**) Entrance slit, (**c**) Exit slit, and (**d**) Image plane. Ray tracing performed for 61 Å, 1800 gr/mm grating and for slit settings of 3 mm × 0·5 mm.

visualize actual intensity distributions on all optical elements and on the image planes, and to check the sensitivity of misalignment and shape variations of the optical elements. For this purpose, the ray tracing program RAY [13] has been adopted on the unix based Magnum mini computer in our institute. The program computes the propagation of a photon beam through an optical system. It simulates the SR emitted from a bending dipole magnet of the synchrotron radiation source and traces a set of pseudo random rays through the optical system to find out the intensity reflected and the intensity distribution at various optical elements. The rays are generated statistically taking into consideration the various storage ring parameters such as bending magnet radius, energy of stored electrons, and vertical and horizontal divergences. The values of these parameters for Indus-1 given in table 1 have been used in ray tracing calculations. The beam line optical layout is also specified as an input to the RAY program. These include the object and image distances for the mirrors and the grating, the surface shapes and sizes, incident and reflection/diffraction angles, and the slit sizes, etc. Various parameters of the optical components given in tables 2 and 3 are employed for ray tracing calculations. The ray trace output consists of points on a plot where each ray intersecting a given plane is plotted.

Figure 2a shows a simulation of the bending magnet source using 1000 rays. Figures 2b, 2c and 2d show the image patterns of this source as taken on the entrance slit, exit slit and the image plane, respectively. These results are for 61 Å, the critical wavelength of Indus-1 and the optical elements are assumed to be perfect without any tangent errors. This figure shows that the source is sharply focused at the image plane. The width of the image in the vertical direction at image plane includes the aberrations of the whole system as well as the contributions due to the finite size of the entrance and exit slits. The full width at half maximum (FWHM) of the image in the vertical direction then gives the overall resolution limit of the beam line. A typical intensity profile in the vertical (dispersive) direction at the image plane is shown in figure 3.

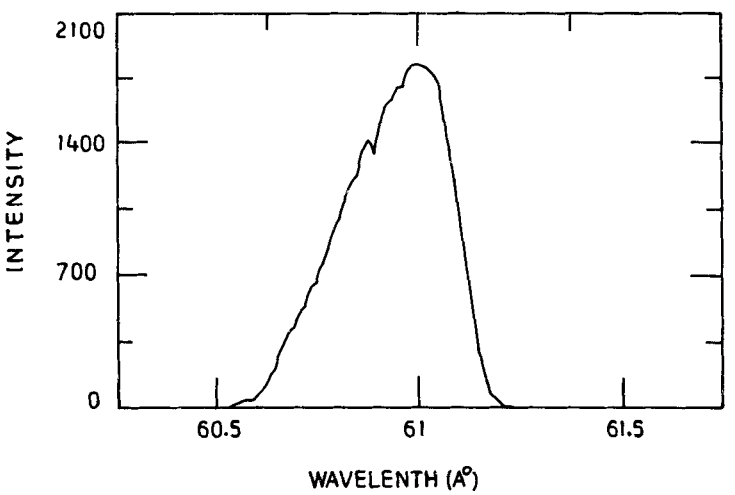

Figure 3. Intensity profile in the vertical (dispersive) direction at the image plane for 61 Å and slit settings of 3 mm × 1 mm.

4.2 *Resolution characteristics*

The resolution achieved by a monochromator in a beam line depends on several factors including the SRS beam size, the photon beam size (S1) at the entrance slit in the dispersive direction, the exit slit size (S2) in the dispersive direction and the geometrical aberration limit of the monochromator. Since our design of TGM utilizes entrance and exit slits at fixed locations the resolution becomes dependent on the wavelength. The attainable resolution of the monochromator is determined by ray tracing as exact analytical evaluation of the various contributions to the resolution is not possible.

In figure 4, the resolution calculated from ray tracing is shown for high energy grating ($N = 1800$ gr/mm) for different slit widths of 200, 500 and 1000 μm. The slit height, which does not influence the resolution, is kept at 3 mm. It can be seen from the figure that for a slit width of 200 μm the resolution is about 0·14 Å between 40 and 120 Å yielding a resolving power ($\lambda/\Delta\lambda$) of 250–700 in this wavelength range. Similar values of the resolving power are obtained for $N = 200$ and $N = 600$ gr/mm gratings. These limiting resolution values have been obtained at slit settings of 200 μm in the dispersive direction which results in a considerable loss of throughput. At higher slit settings, the throughput gets improved significantly though it is at a substantial deterioration of resolution. Theoretically, resolution can be further improved by a factor of 2–4 by masking the outer portions of the grating, since focusing aberrations of the grating limit the resolution rather than the total number of illuminated lines. Horizontally and vertically adjustable apertures are planned to be placed in the entrance arm of the TGM to mask the various regions of the grating. These apertures will also help in reducing the stray light. Furthermore, entrance and exit slits will be continuously adjustable (0–2 mm) in the dispersive direction. In the perpendicular direction also the slits will have adjustable aperture. The effect of the variation of slit widths and the grating masking on the spectral resolution has been systematically investigated and will be reported elsewhere [14].

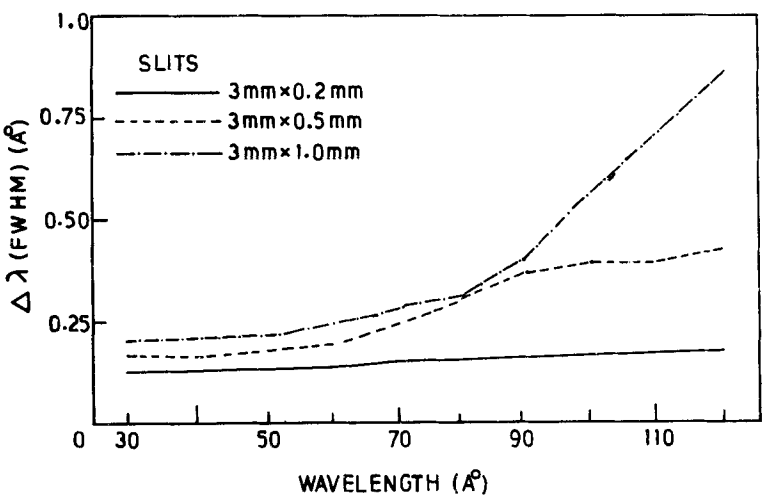

Figure 4. Theoretical resolution curves from ray tracing calculations for different slit setting for 1800 gr/mm grating.

4.3 *Photon flux*

Another parameter of immense interest for experiments using monochromatic light is the maximum photon flux that can be expected on the sample under investigation for a given slit size (or resolution). The flux emitted by the SRS gets attenuated by the beam line because of its nonunity transmission. The transmission is defined as the ratio between the number of rays per unit bandwidth at the image plane and the number of rays per unit bandwidth emitted by the source. It is determined by the pre- and post-focusing mirrors through their reflectivities and dimensions, by the grating through its reflectivity and diffraction efficiency, and by the slit sizes.

Large atomic number elements give substantially higher reflectivities at grazing incidence, nickel being one of the rare exceptions [15]. Platinum, gold or nickel are generally coated on optical elements in the soft X-ray beam lines on SR facilities to get high reflectivity. The reflectivities of these elements are readily calculated using the well documented optical constants data [16, 17]. The reflectivities of these elements at a grazing angle of 4·5° (the grazing angle on toroidal mirrors employed in our beam line) are given in figure 5. This figure shows that gold has higher reflectivity in the 40–300 Å wavelength range, with platinum being marginally worse. Nickel though has a flat response in the wavelength range of our interest, its reflectivity is about 20% lower than that of gold or platinum. We have performed calculations above 300 Å also, and have found that the three elements give almost similar reflectivities in the 300–1000 Å region. Thus, gold is the preferred coating material for the optical elements employed in our beam line.

The grating efficiency is generally measured experimentally as the grating profile parameters required to determine grating efficiency theoretically are not available for the commercially available gratings. However, to get a first order estimate, we have determined the grating efficiency following the procedure outlined by Hellwege [18]. For this, lamellar gratings of groove density (N) of 200, 600 and 1800 grs/mm were taken. To obtain a high diffraction efficiency over a large wavelength range, the grating depth (h) to grating spacing ($1/N$) ratio should have a proper value. After

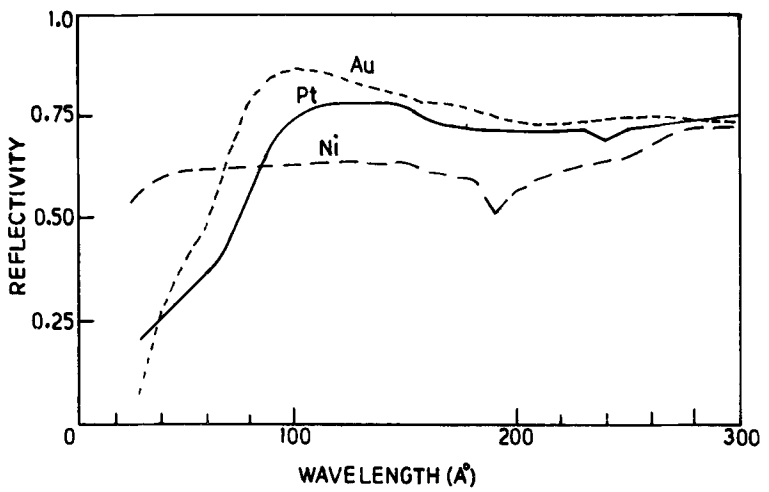

Figure 5. Reflectivities of gold, nickel and platinum at a grazing angle of 4·5°.

performing calculations for grating efficiency for various values of this ratio, we found out that a value of 0·015 gives the best diffraction efficiency in the wavelength range of our interest for three gratings. On the basis of these calculations a maximum of $\sim 40\%$ grating efficiency is achieved in the middle of the wavelength range of each grating. Furthermore, to get an accurate idea of the grating throughput, the reflectivity of the grating substrate should also be considered. We have determined the grating reflectivity in a manner similar to the one used for calculating the reflectivities of mirrors with the only difference that proper account has been taken of the varying angle of incidence over the wavelength scan.

The geometrical throughput and the wavelength bandpass of the beam line has been determined through ray tracing. The geometrical throughput of the beam line is wavelength dependent and it reduces as the wavelength increases because of two counts. One, the vertical divergence of the SRS increases with increasing wavelength and second, the grating incidence angle varies with the wavelength scan. Both these factors result in a net loss of geometrical throughput. Our ray tracing results show that the geometrical throughput reduces from 63% to 25% for $N = 1800$ gr/mm grating, from 54% to 16% for $N = 600$ gr/mm grating, and from 41% to 13% for $N = 200$ gr/mm grating as the wavelength is scanned from the minimum to the maximum of each grating's useful wavelength range. The number of rays generated for ray tracing varied from 20,000 to 200,000 depending upon the wavelength, so as to get good statistics at the image plane in each case. To determine the bandpass, intensity profile of the image in the vertical direction was determined through ray tracing at various wavelengths and the FWHM of this profile was taken to represent the band pass.

Following the above considerations, the photon flux has been determined. Figure 6 shows the absolute number of monochromatic photons which will be available at sample with Indus-1 operating at 450 MeV and 100 mA. The calculations have been performed for 10 mrad horizontal acceptance, for slit settings of 3 mm × 0·5 mm, and for gold coating on optical elements. The figure shows that for these typical

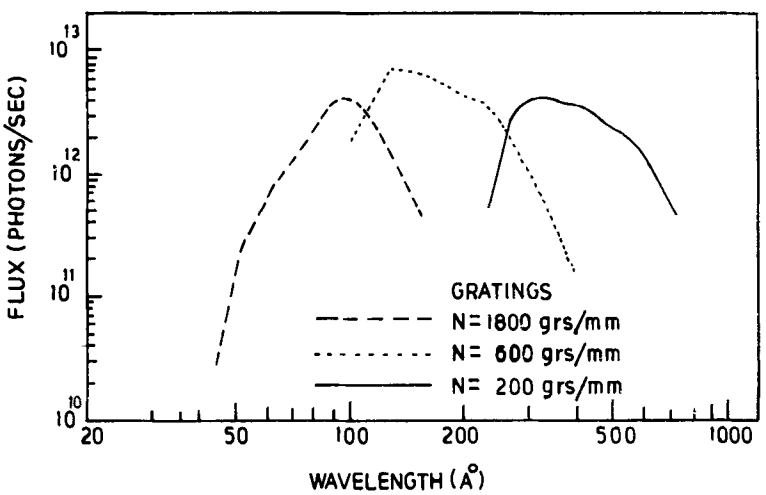

Figure 6. Photon flux as a function of wavelength for all the three diffraction gratings. Calculations have been performed for 10 mrad horizontal acceptance, 100 mA Indus-1 current and slit settings of 3 mm × 0·5 mm.

parameters, photon flux of well over 10^{12} photons/sec can be obtained. At the critical wavelength (61 Å) of Indus-1, one obtains a photon flux of $\sim 8 \times 10^{11}$ photons/sec. Comparing this figure with the number of photons emitted by Indus-1 into the beam line results in a beam line transmission of $\sim 3\%$.

4.4 *Surface figure errors*

The imperfections in the optical elements can severely limit their performance. The acceptable tolerances in the surface figure errors should be evaluated and the mirrors and gratings employed in the beam line should conform to these limits. The main performance limiting imperfections of an optical element are the tangential slope error and the surface micro roughness. While the former deteriorates the resolution, the latter leads to diffused scattering thereby limiting the specular reflectivity. According to Beckmann and Spizzichino [19] the attenuation of the reflectivity due to rms surface roughness of σ is given by an expression of the Debye-Waller form:

$$R = R_0 \exp - \left(\frac{4\pi\sigma \sin \phi}{\lambda} \right)^2 \tag{9}$$

where R_0 is the smooth-surface reflectivity, R is the attenuated reflectivity and ϕ is the glancing angle. This expression indicates that the surface micro roughness greatly limits the performance of optical elements at short wavelengths and large grazing angles. It is readily seen from this expression that a rms surface roughness of 30 Å on the toroidal mirrors (glancing angle = 4·5°) employed in our beam line will lead to about 40% attenuation in reflectivity.

The effect of tangential slope error has been evaluated in the following way. The presence of a tangential slope error of δ in the given surface element of the mirror can be represented as a deviation of the normal to the surface from the optimal direction by δ, which results in the reflected ray rotating by 2δ. This leads to an increase in the spot size by $2\delta r_2$ where r_2 is the image distance from the mirror. This increase in the spot size should not be greater than the aberration limited spot created by the mirror. To determine the aberrated focal spots created by the toroidal pre and post-mirrors, these mirrors were ray traced individually. The mirrors were assumed to be illuminated by a point source and the acceptance of the pre-mirror was taken to be 10 mrad × 5·9 mrad and that of post-mirror to be 20 mrad × 11·7 mrad. All other parameters were taken to be the same as employed in our beam line (figure 1). The results are shown in figures 7a and 7b for pre-mirror and post-mirror, respectively. From the spot diagrams given in these figures it can be seen that the tangential aberrations are respectively of the order of 550 μm and 100 μm for the two mirrors. These values put a limit of 25 arcsec and 6 arcsec on the tangential slope error tolerable for the pre- and post-mirrors employed in our beam line, respectively.

Extending these arguments for the case of a grating results in a wavelength dependent contribution to the resolution from the tangential slope error, as has been derived by Williams [20]. However, Padmore [21] has shown that a tangential slope error of δ in the grating will lead to a wavelength independent contribution to the resolution given by

$$\Delta\lambda = \frac{2\delta \cos \theta}{Nk}. \tag{10}$$

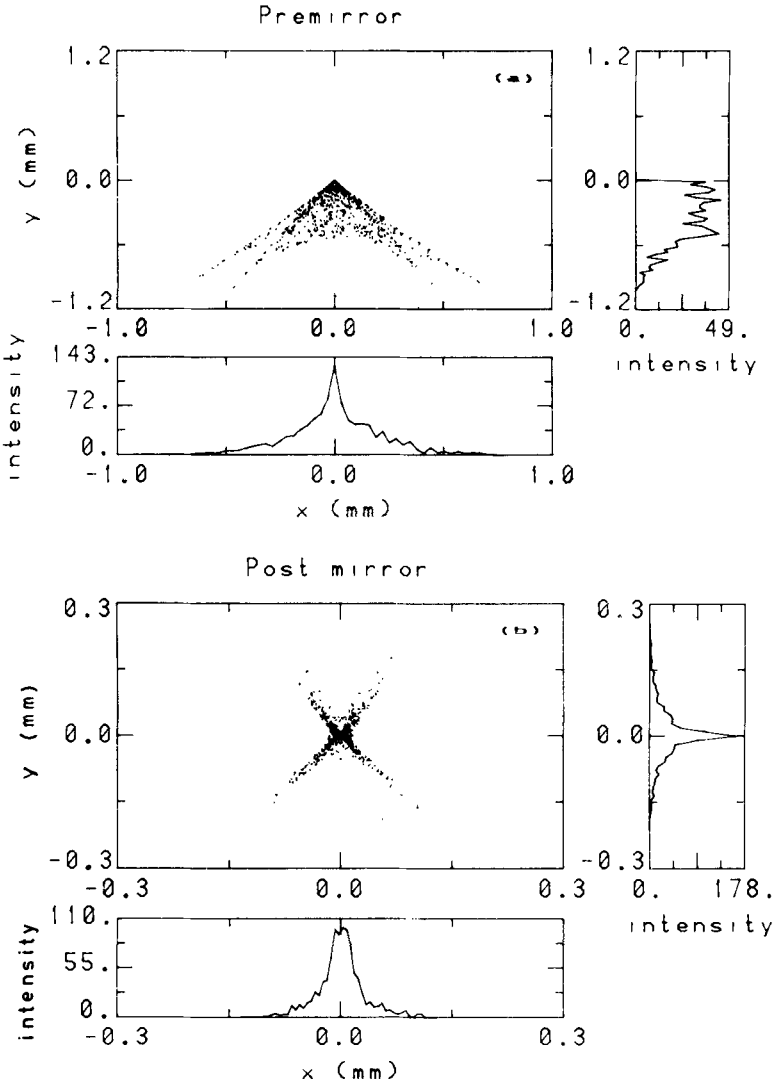

Figure 7. Aberrated focal spots generated by (**a**) pre-mirror and (**b**) post-mirror, when ray traced for point source.

An estimate of the tolerable tangential slope error in the grating can be found out from this equation. It is seen that for a resolving power ($\lambda/\Delta\lambda$) of ~ 1000, the grating should not have a tangential slope error greater than 5 arcsec. The sagittal slope error is seen to have no significant effect on the image quality.

4.5 *Misalignment effects*

The beam line performance can get severely degraded due to incorrect adjustment of optical elements and/or variation in their shapes. To check the sensitivity to misalignment and shape variations of the optical elements ray tracing calculations have been performed at values other than the optimum. The details of these calculations will be reported elsewhere [22]. As a representative case, figure 8 shows the effect

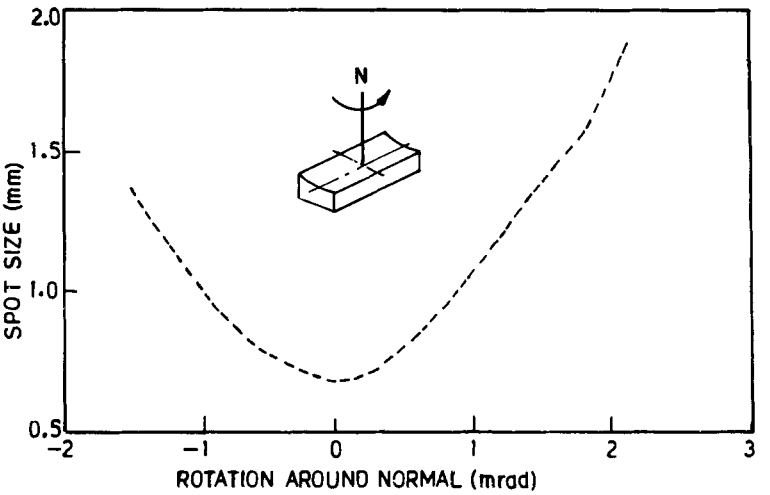

Figure 8. Variation of the spot size created by a single mirror as a function of the adjustment of the mirror in its own plane. The ray tracing calculations have been performed for 61 Å.

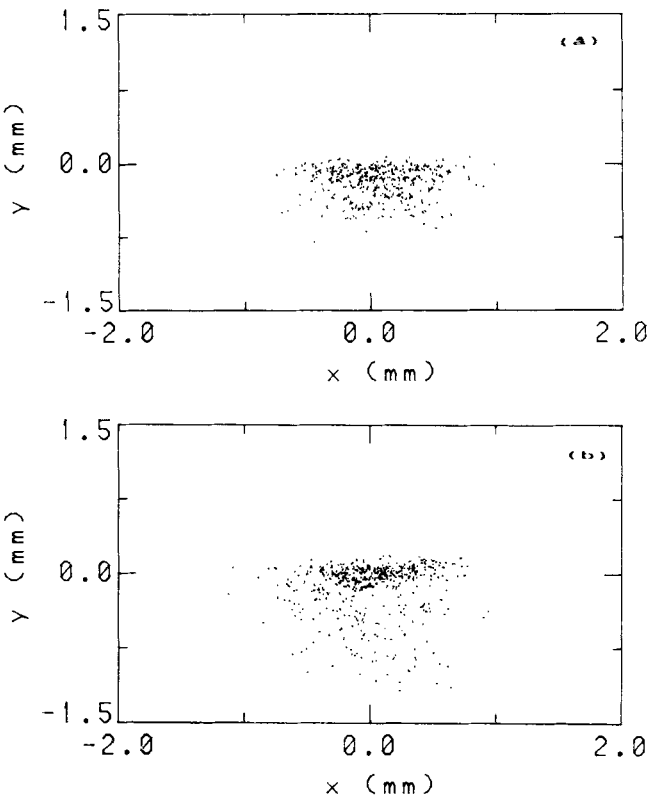

Figure 9. Spot diagram at the focus point of a toroidal mirror: (**a**) Ray traced for a dipole SRS source, (**b**) same as (a) but with a misorientation of the mirror in its plane of 1 mrad.

on spot size at the focusing plane of a single toroidal mirror due to the rotation of the mirror in its plane around an axis perpendicular to its surface. Figure 9a shows the spot diagram obtained from a single mirror with no misalignment errors and figure 9b shows the change in the extent and shape of the focal spot when the mirror is rotated by only 1 mrad. Thus it is evident from figures 8 and 9 that the spot size gets drastically enlarged with only small rotations. Therefore, very fine mechanical controls are being provided [23] in the beam line hardware to permit *in situ* adjustment of the optical elements for optimizing the beam line performance.

5. Summary

Detailed optical design of a TGM-based beam line for Indus-1 storage ring has been described. This beam line will operate in the 40 to 1000 Å wavelength range. The performance of the beam line has been evaluated using ray tracing calculations. The ray tracing results show that a design comprising of proper choice of toroidal pre and post-focusing mirrors and a set of toroidal gratings give optimum performance in terms of resolution and photon flux. Since the beam line has a pre-focusing mirror and an entrance slit, the resolution of the instrument is essentially independent of the source size and the position of the stored electron beam in the SRS. Our calculations show that the beam line will produce a final spot size at the sample of about 2 mm × 0·5 mm and a photon flux of $> 10^{12}$ photons/sec (at 100 mA Indus-1 current).

The effect of various parameters, which may limit the performance of the beam line, has been studied in detail. These include the effect of varying the slit sizes, masking the gratings, presence of surface imperfections and misalignment errors. Also, the resolution of the instrument is wavelength dependent and we have observed that it deteriorates considerably at the high wavelength end of each gratings scan limit. Therefore, to further improve the resolution characteristics, we plan to use, instead of straight groove, constant spacing gratings, the aberration corrected holographically ruled gratings which are commercially available.

This paper gives a reasonable idea about the characteristics of the SR beam, in respect of resolution, photon flux and spot size, which will be available for the users from this beam line and will aid the experimenters to plan their experiments on this beam line.

Acknowledgements

We wish to express our sincere thanks to Dr F Schafers of BESSY for kindly providing the source code of RAY program which enabled us to implement this code on our computer system. We also thank Dr G S Lodha for many useful discussions.

References

[1] R V Nandedkar, K J S Sawhney and G S Lodha, *CAT Report CAT/I/92–01* (1992)
[2] K J S Sawhney and R V Nandedkar, *Proc. Int. Conf. on synchrotron radiation sources*, Indore, India 3–6 Feb 1992, edited by S S Ramamurthi, G Singh and D Angal, 355
[3] G Singh, G K Sahoo, B Singh, D Angal and S S Ramamurthi, *Proc. Internat. Conf. on Synchrotron Radiation Application*, May 9–12, 1989, Hefei, China, edited by H Winick *et al* (Press of Univ. of Science and Technology, Hefei, 1990) 122

[4] R V Nandedkar, *Proc. Int. Conf. on synchrotron radiation sources*, Indore, India 3–6 Feb 1992, edited by S S Ramamurthi, G Singh and D Angal, 279
[5] G Singh, *Private communication* (1990)
[6] D Korsch, *Reflective optics* (Academic Press, Boston, 1991)
[7] K J S Sawhney and R V Nandedkar, *Pramana – J. Phys.* **39**, 177 (1992)
[8] R L Johnson, *Nucl. Instrum. Methods* **A246**, 303 (1986)
[9] H A Padmore, *Rev. Sci. Instrum.* **60**, 1608 (1989)
[10] J B West and H A Padmore, in *Handbook of synchrotron radiation* edited by G V Marr (North-Holland, Amsterdam, 1987) Vol 2, p. 21
[11] W R Mckinney and M R Howells, *Nucl. Instrum. Methods* **172**, 149 (1980)
[12] Personal communication with mirror fabricators
[13] J Feldhaus and F Schafers, *Technical Report BESSY TB-xx-87* (1987)
[14] K J S Sawhney and R V Nandedkar, *to be published* (1994)
[15] V Saile, *SPIE Proceedings* **733**, 126 (1986)
[16] B L Henke, J C Davis, E M Gullikson and R C C Perera, *Lawrence Berkeley Lab. Report LBL-26259* (1988)
[17] E D Palik, *Handbook of optical constants of solids* (Academic Press, Orlando, 1985)
[18] K H Hellwege, *Z. Phys.* **106**, 588 (1937)
[19] P Beckmann and A Spizzichino, *The scattering of electromagnetic waves from rough surfaces* (Pergaman, New York, 1963)
[20] G P Williams, *Nucl. Instrum. Methods* **A246**, 294 (1986)
[21] H A Padmore, *SPIE Proceedings* **733**, 253 (1986)
[22] K J S Sawhney and R V Nandedkar, *to be published* (1994)
[23] A Verma, K J S Sawhney and R V Nandedkar, *Proc. DAE Solid State Phys. Symp.* **C35**, 89 (1992)